Superconductivity under high pressure in the binary compound $CaLi_2$

M. Debessai, T. Matsuoka,* J. J. Hamlin, A. K. Gangopadhyay, and J. S. Schilling
Department of Physics, Washington University, CB 1105, One Brookings Drive, St. Louis, Missouri 63130, USA

K. Shimizu
KYOKUGEN, Center for Quantum Science and Technology under Extreme Conditions, Osaka University, 1-3 Machikaneyama, Toyonaka, Osaka 560-8531, Japan

Y. Ohishi
Japan Synchrotron Radiation Research Institute (JASRI)/SPring-8, 1-1-1 Kouto, Sayo, Hyougo 679-5198, Japan
(Received 6 September 2008; revised manuscript received 28 November 2008; published 30 December 2008)

Feng *et al.* predicted for $CaLi_2$ highly anomalous properties with possible superconductivity under very high pressures, including for the hcp polymorph a significant lattice bifurcation at pressures above 47 GPa. More recently, however, Feng suggested that for pressures exceeding 20 GPa $CaLi_2$ may dissociate into elemental Ca and Li. Here we present for hcp $CaLi_2$ measurements of the electrical resistivity and ac susceptibility to low temperatures under pressures as high as 81 GPa. Pressure-induced superconductivity is observed in the pressure range of 11–81 GPa, with T_c reaching values as high as 13 K. X-ray diffraction studies to 54 GPa at 150 K reveal that hcp $CaLi_2$ undergoes a structural phase transition above 23 GPa to orthorhombic but does not dissociate into elemental Ca and Li. In the hcp phase a fit of the equation of state with the Murnaghan equation yields the bulk modulus $B_o=15(2)$ GPa and $dB_o/dP=3.2(6)$.

DOI: 10.1103/PhysRevB.78.214517 PACS number(s): 74.70.Ad, 74.10.+v, 74.25.Dw, 74.62.Fj

I. INTRODUCTION

Of the 30 elemental metals in the Periodic Table which superconduct at ambient pressure, 10 are simple s,p-electron metals, whereas the remaining 20 have a conduction band dominated by d electrons.[1] In d-electron superconductors the sign of the pressure dependence of the superconducting transition temperature dT_c/dP may be either positive or negative; in contrast, in simple-metal superconductors T_c is found, without exception, to initially *decrease* under pressure.[1] In fact, in the very first high-pressure measurement ever carried out on any superconductor, a negative value of dT_c/dP was observed for Sn by Sizoo and Onnes[2] in 1925. It follows that nonsuperconducting simple metals, such as the alkali metals Na, K, Rb, Cs, and all alkaline earths, would *not* be expected to become superconducting under high pressure. Li has recently been reported to superconduct at very low temperatures (~0.4 mK) (Ref. 3); one would anticipate that Li's T_c will decrease to even lower temperatures should high pressures be applied. It is thus remarkable that under extreme pressures Li, Cs, Ca, Sr, and Ba become good superconductors with *positive* dT_c/dP, where T_c reaches values as high as 14 K for Li (Refs. 4–6) and 25 K for Ca,[7] the latter a record high value for an elemental superconductor which surpasses that of all known A-15 compounds, the record holders before the discovery of the high-T_c oxides in 1986.

The robust superconducting state of the alkali- and alkaline-earth metals under very high pressures thus contradicts the expectations for a simple metal. The same is true of the electrical resistivity ρ of Ca (Ref. 7) and Li,[4,8] for example, which is found to increase strongly under pressure, in contrast to the negative $d\rho/dP$ dependence found for simple metals, such as Cu,[9] arising mainly from the increase in the Debye temperature with pressure. In addition, contrary to the textbook expectation that the crystal structures assumed by a simple metal become more highly symmetric under pressure, the crystal structures of both alkali metals and alkaline earths become *less* symmetric, another signature of their anomalous properties. The behavior of the alkali metals under high pressure has been recently reviewed.[10]

Why do simple metals lose their "simplicity" under very high pressures? Neaton and Ashcroft[11,12] showed that the electronic properties of Li and Na are expected to become anomalous if the pressure is sufficiently high to bring neighboring ion cores into near contact. In this situation the conduction electrons, whose wave functions must be orthogonal to the core states, must avoid the core region and thus are confined mainly to the interstitial sites. At very high pressures the conduction bandwidths in Li,[11] Na,[12] and Ca (Ref. 13) actually decrease under pressure, a counterintuitive result. Very recent work of Rousseau and Ashcroft,[14] in fact, has shown that this bandwidth narrowing is a direct result of the increasing localization of the conduction electrons as they are trapped in the interstitial sites between the ion cores. Associated with this localization is a strong enhancement of p and/or d admixture into the conduction band, an effect pointed out many years ago by Vasvari *et al.*[15] for Ca, Sr, and Ba under pressure.

The rationale given for the anomalous electronic properties of simple metals under strong compression, namely, the increasing conduction-electron localization into interstitial sites, may have a much wider range of validity, perhaps applying to compounds and alloys of simple metals and possibly even transition metals.[12,14] The first step in exploring this question would be to study a simple-metal binary compound where each of the constituent elements themselves has been shown to exhibit anomalous behavior under pressure. In view of the above discussion of Li and Ca, the Laves-phase compound $CaLi_2$, the only known compound between Li and

Ca, would appear to be the ideal choice. Feng *et al.*[16] carried out detailed electronic structure calculations on both the hexagonal and cubic forms of $CaLi_2$ and found that indeed the electronic properties and structural sequences become, as for Li and Ca, markedly anomalous under pressure, with superconductivity a likely possibility. They predict that for hexagonal $CaLi_2$ this symmetry is maintained to over 200 GPa, with, however, a significant lattice bifurcation at pressures above 47 GPa. On the other hand, more recent work by Feng[17] reveals that $CaLi_2$ becomes thermodynamically unstable above 20 GPa and should dissociate into elemental Ca and Li, if the kinetics allow.

In a recent paper we reported pressure-induced superconductivity in $CaLi_2$ for pressures above 11 GPa, whereas at ambient pressure this compound does not superconduct above 1.10 K.[18] In the present paper we report extensive measurements of the electrical resistivity ρ, ac susceptibility χ', and crystal structure of hexagonal $CaLi_2$ in polycrystalline form at both ambient and high pressures. The electrical resistivity is found to increase strongly under pressure over the entire temperature range below 298 K. A superconducting transition appears in both $\rho(T)$ and $\chi'(T)$ under pressure where T_c reaches values near 13 K at ~40 GPa. The equation of state and linear compressibilities are determined to 24 GPa.

II. EXPERIMENTAL

The starting materials for the synthesis of $CaLi_2$ were crystalline dendritic pieces of Ca with stated purity 99.98% (metals basis) from Alfa Aesar and 99.99% Li rod (metals basis) from ESPI Metals. Magnetic measurements [vibrating-sample magnetometer (VSM), Quantum Design, 2–300 K, 0–6 T] on the starting materials gave an Fe-equivalent impurity concentration for Ca of 9 and 30 (atomic) ppm from the saturation magnetization and the Curie tail, respectively. Corresponding measurements on Li gave 20 and 9 ppm, whereas for the $CaLi_2$ compound 15 and 20 ppm were obtained.

The $CaLi_2$ sample was prepared by melting together stoichiometric amounts of Ca and Li in a stainless-steel crucible placed on a hot plate located in an Ar-gas glovebox. Because the sample slightly wet the stainless steel, a 13-μm-thick Ta foil was cupped and placed between the sample and crucible and a Ta rod was used to stir the molten sample for approximately 30 min at a temperature somewhat above the melting temperature of $CaLi_2$ (235 °C); there is no known chemical reaction between Li or Ca and Ta at this temperature. The crucible was then removed from the hot plate, and the sample was allowed to cool to ambient temperature. A sample prepared in this way will be called henceforth "sample A." A measurement of the electrical resistivity $\rho(T)$ yielded the residual resistivity ratio (RRR) $\rho(298\ \mathrm{K})/\rho(2\ \mathrm{K}) \simeq 170$, a relatively high value for an intermetallic compound.

In preparation for x-ray powder-diffraction studies, the sample was ground to a powder in an agate mortar and pestle in the Ar glovebox, placed together with a small amount of Si marker onto a 20×20 mm^2 square area on a glass slide, covered with a 10-μm-thick poly vinyl film and sealed shut with putty; this technique yielded a much superior signal/noise ratio in the x-ray pattern compared to our previous work using glass capillaries.[18] The glass slide was placed in a Rigaku Geigerflex D/max-B x-ray diffractometer utilizing Cu K_α radiation ($\lambda = 1.540598$ Å). The diffraction pattern obtained after 5 h for sample A is shown in Fig. 1(a). In Table I the peak positions and relative intensities of the diffraction lines [with respect to the highest intensity (103)] are tabulated and compared with the published data[19] for the hexagonal polymorph of $CaLi_2$. The lattice parameters for the hexagonal unit cell can be estimated to be $a = 6.279(1)$ Å and $c = 10.243(1)$ Å, in reasonably good agreement with the published values $a = 6.248(8)$ Å and $c = 10.23(2)$ Å from Hellner and Laves,[19] $a = 6.268(2)$ Å and $c = 10.219(5)$ Å from Nesper and Miller,[20] and $a = 6.261$ Å and $c = 10.250$ Å from Ref. 21. Scanning electron micros-

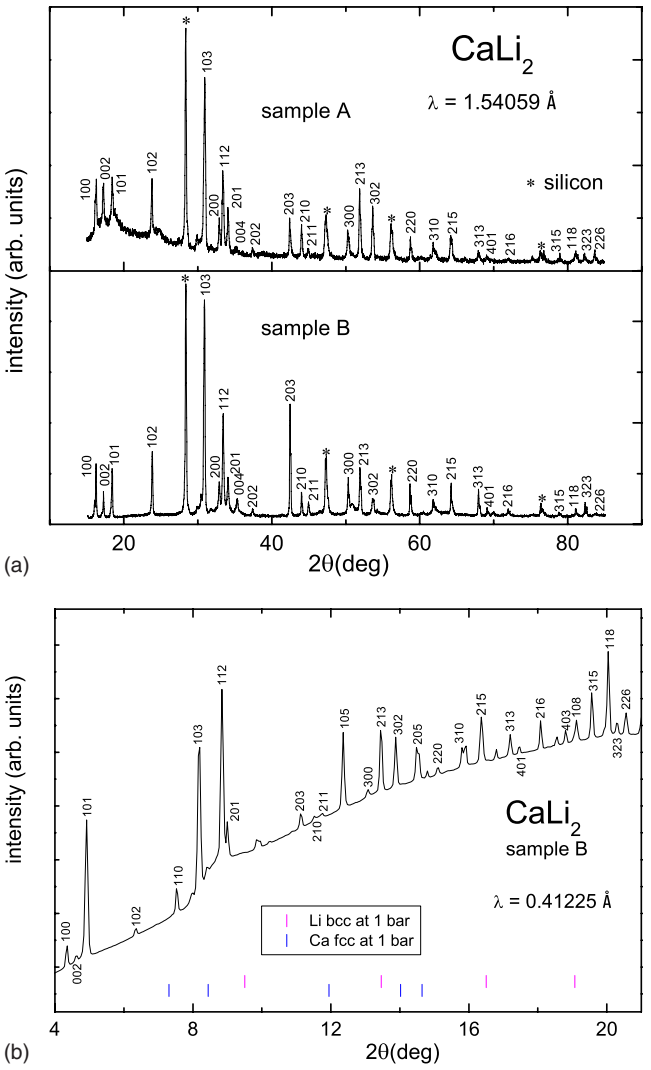

FIG. 1. (Color online) X-ray powder-diffraction pattern for $CaLi_2$ at ambient pressure using a conventional diffractometer: (a) samples A (top) and B (bottom) plus Si marker (*); (b) diffraction pattern from sample B using synchrotron radiation at shorter wavelength. Vertical lines mark expected peak location for bcc Li and fcc Ca.

TABLE I. Results of x-ray powder diffraction for present $CaLi_2$ samples A and B compared to published data. I_{meas} (I_{cal}) is measured (calculated) relative intensity.

	Sample A		Sample B		Ref. 19		
hkl	2θ (deg)	I_{meas}	2θ (deg)	I_{meas}	2θ (deg)	I_{cal}	I_{meas}
100	16.282	1.05	16.248	1.0			
002	17.220	0.95	17.267	0.49			
101	18.445	1.10	18.423	0.91			
102	23.806	1.31	23.850	1.19	23.930	0.4	1–2
110	Si		Si		28.413	2.6	3–4
103	30.943	4.00	30.893	4.00	30.907	3.5	4–
200	32.906	0.72	32.906	0.52			
112	33.420	1.82	33.432	1.78	33.315	3.4	3.5–4
201	34.091	0.96	34.086	0.59			
202	37.374	0.18	37.422	0.13	37.311	0.1	0.5+
203	42.452	0.94	42.492	2.10	42.530	1.9	2++
210	44.022	0.75	44.041	0.43	44.217	0.3	1
211	44.944	0.20	44.985	0.26	45.062	0.2	1–
105	Si		Si		47.589	3.2	2–3
300	50.279	0.66	50.337	0.69	50.537	1.4	2
213	51.877	1.82	51.931	0.88	52.041	4.0	3
302	53.647	1.22	53.694	0.30	53.830	2.1	2+
205	Si		Si		56.452	3.1	2.5
220	58.734	0.54	58.675	0.57	59.027	1.6	2
310	61.811	0.43	61.805	0.29	62.070	1.7	2
215	64.188	0.59	64.232	0.60	64.710	3.8	2.5–3
313	67.918	0.25	67.944	0.48	68.251	2.6	2+
401	69.044	0.14	68.960	0.15			
216	71.972	0.10	71.949	0.14	72.068	0.2	0.5
403	74.000	Weak					Weak
108	Si		Si		76.870	0.3	1–
315	78.930	0.22	78.795	0.24	79.059	0.7	1.5
118	81.081	0.28	81.077	0.14	81.348	1.7	2–
323	82.270	0.22	82.336	0.26	82.565	0.8	1.5+
226	83.660	0.30	83.683	0.05	83.983	1.8	2–

copy (Hitachi S-4500) images, as seen in Fig. 2(a), revealed the presence of a small concentration (<5 vol %) of a Ca-rich impurity phase (brighter regions) which was not visible in the x-ray powder pattern in Fig. 1(a).

To reduce the amount of impurity phase and further improve the sample homogeneity, a second $CaLi_2$ sample was first synthesized in the same way as sample A above but was additionally wrapped in a Ta foil, sealed in a quartz tube filled with Ar, and annealed in a box furnace at a temperature of 210 °C for 24 h. For sample B we found the RRR to be $\rho(298\ \mathrm{K})/\rho(2\ \mathrm{K}) \simeq 43$. The resulting x-ray diffraction pattern is shown in Fig. 1(a) and summarized in Table I, yielding the hexagonal lattice parameters $a=6.280(1)$ Å and $c=10.239(1)$ Å which differ only slightly from those of sample A. The scanning electron micrograph in Fig. 2(b) is seen to be nearly free of the impurity phase seen in Fig. 2(a) for sample A. In a further effort to detect possible impurity phases of unreacted Li or Ca, high-resolution x-ray diffraction data were collected near the most intense peak positions for Li (110) and Ca (200), (220), and (311), well separated from the $CaLi_2$ diffraction lines. This allowed us to estimate the upper limits of these impurity phases, if any, to be below 1.7% (Li) and 0.3% (Ca). To further enhance the experimental resolution, synchrotron-radiation studies were also carried out on sample B, as seen in Fig. 1(b).[22] The absence of any of the above diffraction peaks allowed a further reduction in the estimated impurity limit to ≤0.3% for Li and ≤0.1% for Ca.

High-pressure resistivity and ac susceptibility experiments were carried out using both a Harwood Engineering He-gas pressure system as well as two different types of diamond-anvil cell (DAC), one (type 1) designed by one of

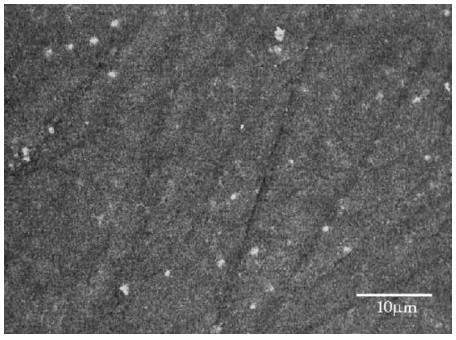

(a)

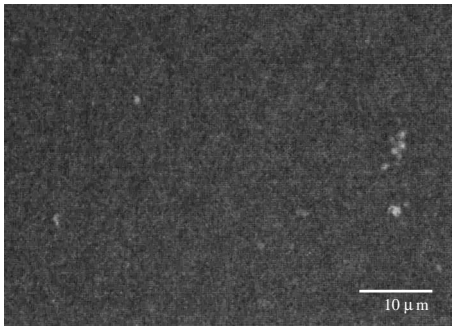

(b)

FIG. 2. Scanning electron micrographs of $CaLi_2$ for: (a) sample A and (b) sample B. Isolated white regions contain a Ca-rich impurity phase. Dark lines in (a) are from sample polishing.

the authors (J.S.S.)[23] and the other (type 2) brought by another author (T.M.) from Osaka University.[24] Both DACs utilize a He-loaded double diaphragm which allows one to change pressure at nearly any temperature below ambient. The type-1 DAC uses two opposing 1/6-carat, type Ia diamond anvils with 0.3 or 0.5 mm diameter culets, whereas the culet diameter in the type-2 DAC, with 1/4-carat type Ib synthetic diamonds, is 0.3 mm. Both Re and W-25 at. % Re gaskets with thickness ~ 250 μm were used in the present measurements. The superconductivity of these gaskets at 4 and 5 K, respectively, restricts the search for superconductivity in $CaLi_2$ in the present ac susceptibility studies to higher temperatures; the electrical resistivity measurement is not affected by the gasket's superconductivity since the electrical leads to the sample are electrically isolated. Tiny ruby spheres[25] are placed on or near the sample to allow the pressure determination using the revised ruby calibration of Chijioke *et al.*[26]

For the electrical resistivity measurements in both the He-gas and DAC high-pressure systems a standard four-point ac technique was used at 13 Hz frequency with a Stanford Research SR830 digital lock-in amplifier. For the measurements in the He-gas system the sample (dimensions $\sim 2.5 \times 6 \times 0.8$ mm^3) is placed on a sample holder into the 7 mm diameter bore of a standard CuBe pressure cell from Unipress. As long as the temperature is above the melting curve of He ($T_{\mathrm{melt}} \simeq 43.6$ K at 0.6 GPa), the pressure is purely hydrostatic. A much smaller sample (diameter ~ 100 μm and 10 μm thick) was used for the resistivity measurements in the DAC where the Pt voltage leads lie approximately 20–30 μm apart. Besides the epoxy/diamond-powder mixture used in the resistivity technique,[27] no pressure medium was used so that the pressure applied to the sample is best characterized as "nonhydrostatic;" the pressure gradient across the sample and the shear stresses on the ruby spheres may, therefore, be appreciable. For example, if the pressure at the sample center is 35 GPa, the pressure at a position 35 μm away is typically reduced by ~ 15 GPa to 20 GPa; the width of the R_1 ruby fluorescence line[28] may be as large as ± 15 GPa. In comparing results from different experiments, therefore, the position of the ruby sphere in the cell should be taken into account.

In the type-1 DAC the ac susceptibility is measured using two compensated primary/secondary coil systems: one around the diamond anvils with sample and the other just outside. The signal from the secondary coils is fed into an SR554 transformer preamplifier connected to an SR830 lock-in amplifier with an applied field of 3 Oe rms at 1023 Hz. ac susceptibility measurements were carried out using either dense He pressure medium (nearly hydrostatic pressure) or no pressure medium at all (nonhydrostatic pressure). In either case the width of the ruby R_1 line is a good deal narrower than in the resistivity studies. Further details of the DAC techniques used in the electrical resistivity[27] and ac susceptibility[23,29] measurements are given elsewhere, as are those for the He-gas compressor system.[30]

For x-ray diffraction studies under high pressure a type-2 DAC (Ref. 24) was used at the SPring-8 Japan Synchrotron Radiation Research Institute, JASRI/SPring-8, Mikazuki, Japan on beamline BL10XU using 0.414 89 Å wavelength radiation.

III. RESULTS OF EXPERIMENT AND DISCUSSION

A. X-ray diffraction studies

In the high-pressure x-ray diffraction studies on $CaLi_2$ (sample A), no pressure medium was used. The results at 2.9, 5.3, 12.8, and 20.2 GPa nonhydrostatic pressure shown in Fig. 3(a) indicate that the hexagonal phase is retained to 20.2 GPa; however, at 12.8 and 20.2 GPa the diffraction peaks have noticeably broadened, perhaps due to pressure gradients or strain effects across the sample.

In their calculations Feng *et al.*[16] found no phase transition away from the hexagonal phase for pressures below 46 GPa. In more recent work, however, Feng[17] anticipated that $CaLi_2$ may dissociate into elemental Ca and Li for $P \gtrsim 20$ GPa. For 0.41489 Å wavelength radiation the dominant (111) diffraction peaks for elemental fcc Ca and Li at 20.2 GPa should lie at $2\theta = 8.759$ and 14.027 degrees, respectively; the (111), (200), and (220) peak locations for Ca are indicated by red arrows in Fig. 3(a). The fact that none of these peaks can be resolved is consistent with the absence of elemental Ca or Li in sample A; i.e., at ambient temperature $CaLi_2$ does not dissociate to pressures as high as 20.2 GPa. This is not too surprising since the present experiments were carried out at a temperature (298 K) which is 210 K below the melting temperature T_m of $CaLi_2$, resulting in slow kinetics. The kinetics may become even slower at high pressures should T_m for $CaLi_2$ increase. Under 8 GPa pressure T_m in-

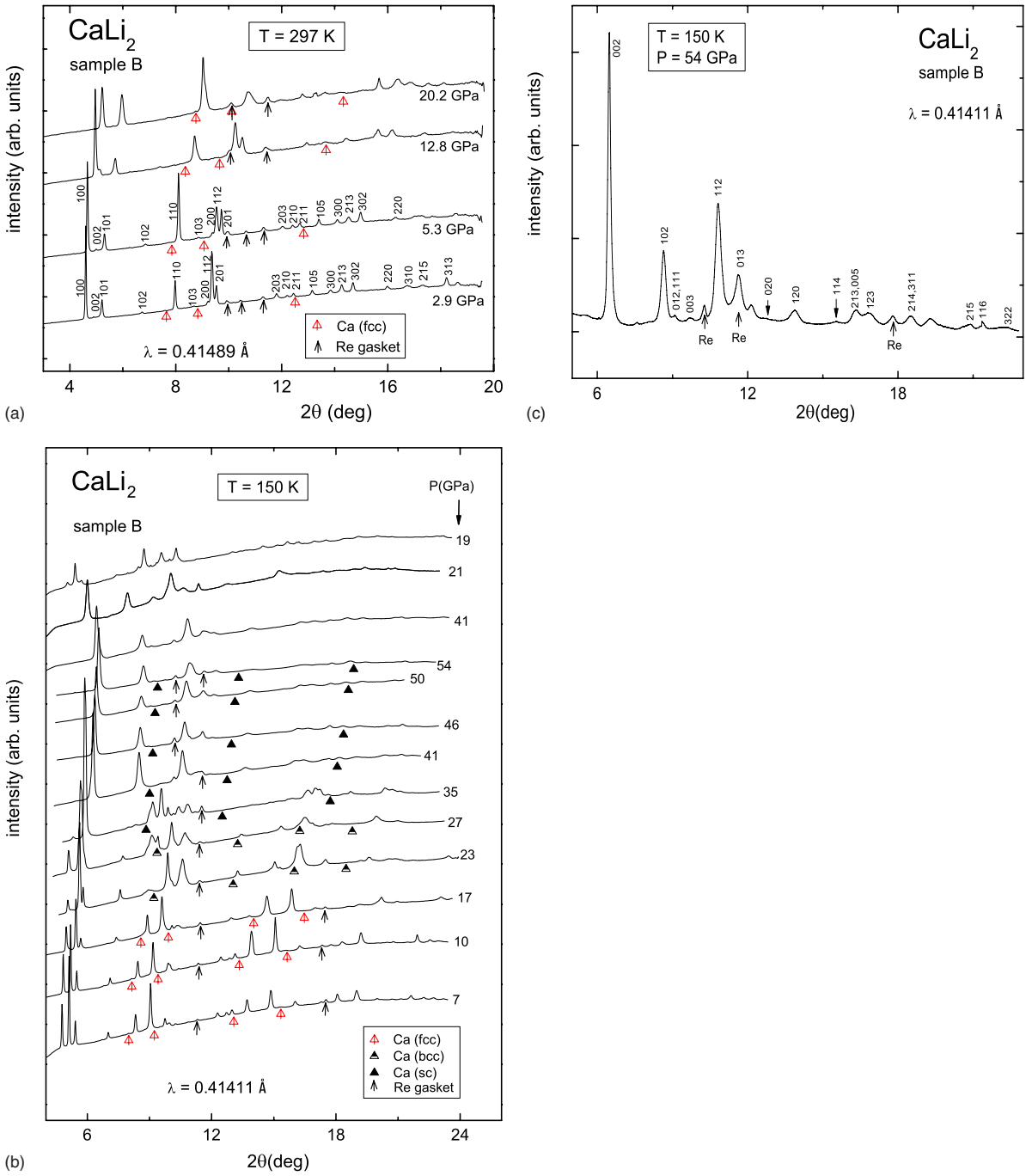

FIG. 3. (Color online) X-ray diffraction pattern for hexagonal $CaLi_2$ using a DAC with synchrotron radiation. Order of measurement is from bottom to top. Vertical black arrows mark location of peaks from Re gasket. (a) Measurements at 297 K on sample A. Peaks are labeled with Miller indices. Vertical open arrowheads mark location of strongest peaks from fcc Ca (111), (200), (220). (b) Measurements at 150 K on sample B. See legend for location of Ca peaks in fcc, bcc, or sc phases at respective pressures (Ref. 33). (c) Diffraction data at 54 GPa with peaks indexed to an orthorhombic phase with lattice parameters a=4.16 Å, b=3.80 Å, and c=7.33 Å. The large background superposed on the diffraction peaks in Fig. 3(b) was subtracted from data to facilitate identification of peaks.

creases from 453 to 530 K for Li (Ref. 31) and from 1112 to 1500 K for Ca.[32]

As we will discuss below, in the search for pressure-induced superconductivity in resistivity and ac susceptibility measurements to 81 GPa on sample B in a DAC, the pressure was changed at low temperatures (<180 K) to avoid a possible reaction of $CaLi_2$ with the diamond anvils. We decided, therefore, to carry out synchrotron x-ray diffraction experiments under similar temperature and pressure conditions on sample B to explore the possibility of structural phase transitions and/or dissociation of $CaLi_2$. The results are given in Fig. 3(b). Following the initial application of 7 GPa pressure at ambient temperature, the sample was cooled to 150 K and kept at that temperature throughout the experi-

ment. Successively higher pressures were applied of 10, 17, 23, 27, 35, 41, 46, 50, and 54 GPa, in that order. For pressures above ~23 GPa, a clear change in the diffraction pattern indicative of a possible phase change is visible; in fact, some subtle changes, such as the disappearance of several diffraction lines with moderate intensities, for example, (112), (300), (213), and (313), started even around 17 GPa. At 27 GPa it is impossible to attribute all the experimental diffraction lines to the hcp phase alone. Careful analysis of the 54 GPa diffraction data [see Fig. 3(c)] reveals that the high-pressure phase is most likely orthorhombic with lattice parameters a=4.16 Å, b=3.80 Å, and c=7.33 Å. Except for a few low intensity peaks (e.g., at 2θ=12.14 or 19.32°), most of the experimental diffraction peaks could be matched to this orthorhombic phase. Forcing the diffraction peaks to fit to the hcp phase left many unidentified peaks; moreover, the a-axis lattice parameter had to be increased to values higher than the corresponding lower pressure data, which is an unrealistic situation. The amount of this orthorhombic phase showed a systematic growth at the expense of the hcp phase as pressure exceeded about 27 GPa, becoming comparable to the hcp phase at ~35 GPa and nearly phase pure above ~46 GPa. Upon releasing pressure to 41, 21, and 19 GPa at 150 K, initially no phase change was observed. However, following an 8 h wait at 19 GPa, during which time the DAC and sample warmed up to ambient temperature, a substantial fraction of the sample reverted back to the original hexagonal Laves phase. The data shown in Fig. 3(b) at 19 GPa were taken after cooling back to 150 K; at all temperatures between 150 K and ambient, the pressure remained in the range of 19–20 GPa. These results indicate that the pressure-induced phase transformation is reversible and, most likely, kinetically hindered at temperatures near 150 K. Interestingly, the absence of the anticipated x-ray diffraction peaks for the fcc, bcc, and sc Ca phases[33] during this transformation, indicated by the vertical arrows in Fig. 3(b), is good evidence that $CaLi_2$ does not dissociate into elemental Ca and Li to pressures up to 54 GPa at 150 K. The observed phase transformation to a lower symmetry phase under pressure in this alkali-metal compound, although counterintuitive, is similar to the many other anomalous properties observed for elemental alkali metals,[10] as will be repeatedly emphasized in this paper.

In Fig. 4(a) hexagonal lattice parameters a and c for $CaLi_2$ plus ratio c/a are plotted versus pressure to 24 GPa. The solid lines are fits to the data given by the equations

$$a(\text{Å}) = 6.24(5) - 0.082(11) \times P + 0.0017(4) \times P^2,$$

$$c(\text{Å}) = 10.22(9) - 0.16(2) \times P + 0.0032(8) \times P^2,$$

$$c/a = 1.64(3) - 0.0038(14) \times P, \quad (1)$$

where P is given in units of GPa. The equation of state V/V_o to 24 GPa is shown in Fig. 4(b) and is fit using the Murnaghan equation[34]

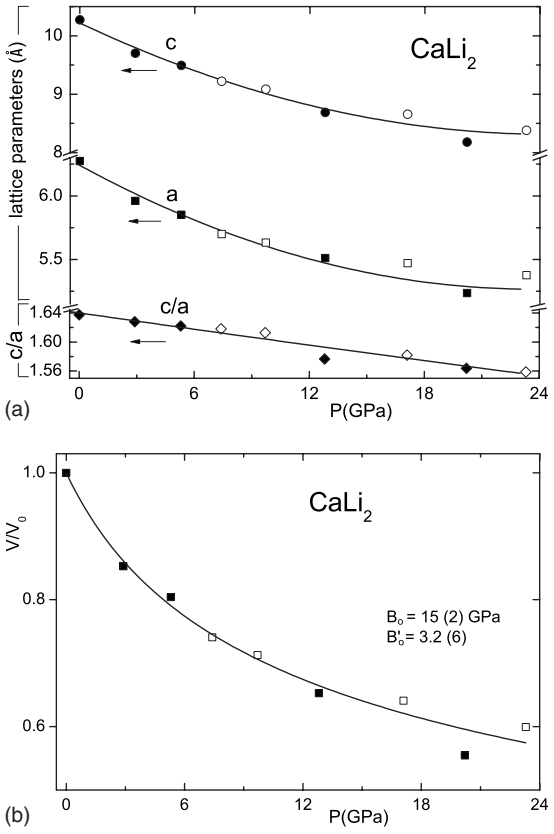

FIG. 4. (a) Hexagonal lattice parameters a and c plus c/a versus pressure to 24 GPa using hcp data from Fig. 3(a) (■,●) and Fig. 3(b) (□,○) for samples A and B, respectively. Solid lines are data fits given in Eq. (1). (b) Relative unit-cell volume versus pressure. Solid line is fit to data using Murnaghan equation [see Eq. (2)].

$$V/V_o = [1 + (B_o'/B_o)P]^{-1/B_o'}, \quad (2)$$

where V_o=350.21 Å^3 is the molar volume at ambient pressure and the bulk modulus and its pressure derivative are given by $B_o \simeq 15(2)$ GPa and $B_o' \simeq 3.2(6)$, respectively. The equation of state of $CaLi_2$ to 24 GPa is quite comparable to that of Ca (Ref. 33) but lies above that of the more compressible Li.[10,35]

B. Electrical resistivity measurements

1. He-gas compressor system

Figure 5(a) shows the temperature dependence of the electrical resistivity for sample B from 12 to 298 K at both ambient and 0.70 GPa hydrostatic pressures (pressure measured at 150 K); at 298 K the pressure was ~0.09 GPa higher and at 10 K ~0.05 GPa lower than 0.7 GPa. The RRR for this piece of sample B was found to be from Fig. 5(a) $\rho(298\ \text{K})/\rho(12\ \text{K}) \simeq 25$. It is to be noted that the RRR was found to vary considerably from sample to sample taken from the same batch which may be indicative of the presence of microcracks in these brittle materials.

Note the weak negative curvature in $\rho(T)$ for temperatures above 100 K. Under pressure the resistivity increases over the entire measured temperature range. At ambient tempera-

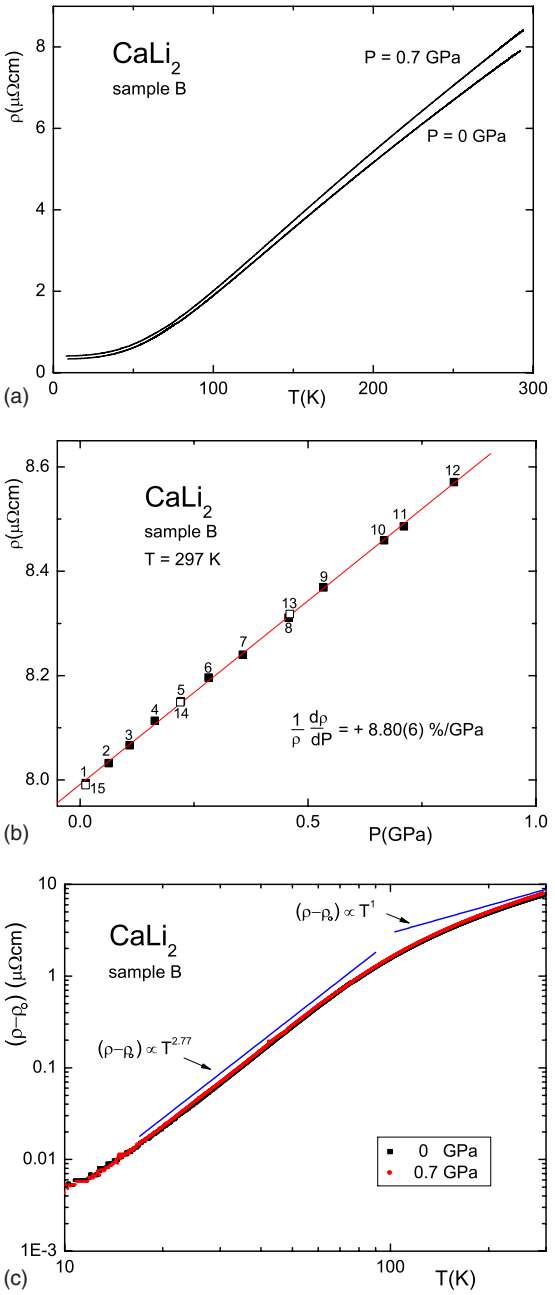

FIG. 5. (Color online) For $CaLi_2$ (sample B): (a) electrical resistivity versus temperature at ambient pressure and 0.70 GPa. (b) Dependence of resistivity at ambient temperature on pressure to 0.72 GPa. Numbers give order of measurement. (c) Log-log plot of temperature-dependent resistivity versus temperature at 0 and 0.7 GPa. ρ_o is the extrapolated residual resistivity (see text). Straight solid lines show power-law dependences $(\rho-\rho_o)\propto T^n$, where $n=1$ and 2.77 at high and low temperatures, respectively.

ture the resistivity is seen in Fig. 5(b) to increase reversibly and linearly with pressure at the rate +8.80(6)%/GPa. To extract the temperature-dependent part of the resistivity, the residual resistivity ρ_o at 0 K is estimated by fitting the data at both pressures from 12 to 60 K using the three-variable equation $\rho(T)=\rho_o+AT^n$; we find $\rho_o\simeq 0.333$ and 0.407 $\mu\Omega$ cm at 0 and 0.7 GPa pressure, respectively, and $n=2.77$ for both. In Fig. 5(c) we plot $[\rho(T)-\rho_o]$ on a log-log plot. Whereas at temperatures below 80 K the data are fit quite accurately by $(\rho-\rho_o)\propto T^{2.77}$, at higher temperatures the data appear to bend over and approach the $(\rho-\rho_o)\propto T^1$ dependence anticipated according to the Bloch-Grüneisen law for a free-electron metal at temperatures well above the Debye temperature.[36] We emphasize, however, that the exponent $n=2.77$ at lower temperatures is not consistent with free-electron behavior ($n=5$), giving evidence that the electronic properties of $CaLi_2$ are anomalous. This conclusion is strengthened by the fact that here the resistivity increases under pressure at all temperatures, in contrast to the expectation from the free-electron Bloch-Grüneisen law where $\rho(T)$ would be expected to decrease at all temperatures due to the dominant effect of lattice stiffening, as observed in the elemental metals Cu,[9] Pb,[37] and Sn,[37] where the Debye temperature increases with pressure, with electronic effects playing only a minor role.

2. Diamond-anvil system

The results of the present electrical resistivity measurements on sample B in the DAC to 24 GPa nonhydrostatic pressure are shown in Fig. 6(a). The rapid increase in the resistivity with pressure at all temperatures seen in the "low-pressure" data in Fig. 5 is seen to continue up to much higher pressures. For pressures above 7 GPa the DAC was kept at temperatures below 180 K to reduce the chance that the sample would react with the diamond anvils. At 13.5 GPa a slight decrease in $R(T)$ is seen below 2 K which hints at a superconducting onset. The superconducting transition becomes clear at 20 GPa, with T_c shifting to higher temperatures with pressure. The indicated values of the pressure in this experiment are likely 10–15 GPa too low since the fluorescing ruby sphere was located ~30 μm from the center of the sample (see discussion in Sec. II). Unfortunately, the ruby sphere originally at the sample center could not be detected.

The suppression of the superconducting transition at 24 GPa by ~0.16 K in a 500 Oe magnetic field is shown in Fig. 6(b); the transition was first measured twice at 0 Oe (points 1,2), then twice at 500 Oe (points 3,4), and followed by a final measurement at 0 Oe (point 5). The reproducibility and reversibility of the "fine structure" in the superconducting transition in a magnetic field are quite remarkable.

Using an identical high-pressure resistivity technique, the temperature-dependent resistivity data in Fig. 6(c) were obtained for sample A to nonhydrostatic pressures as high as 81 GPa. As before, the DAC was kept at a temperature below 180 K following the initial application of 8 GPa pressure at ambient temperature. Here also, the resistivity increases rapidly with pressure over the entire measured temperature range. That the resistivity enhancement with pressure is reasonably reversible is demonstrated by the final measurement at 46 GPa where $R(T)$ is seen to lie well below the dependence for 81 GPa. In this measurement the pressure was determined from a ruby sphere located at the sample center. Exact reversibility of the resistivity is not expected in this measurement considering the brittleness of the material and the nonhydrostatic pressure conditions.

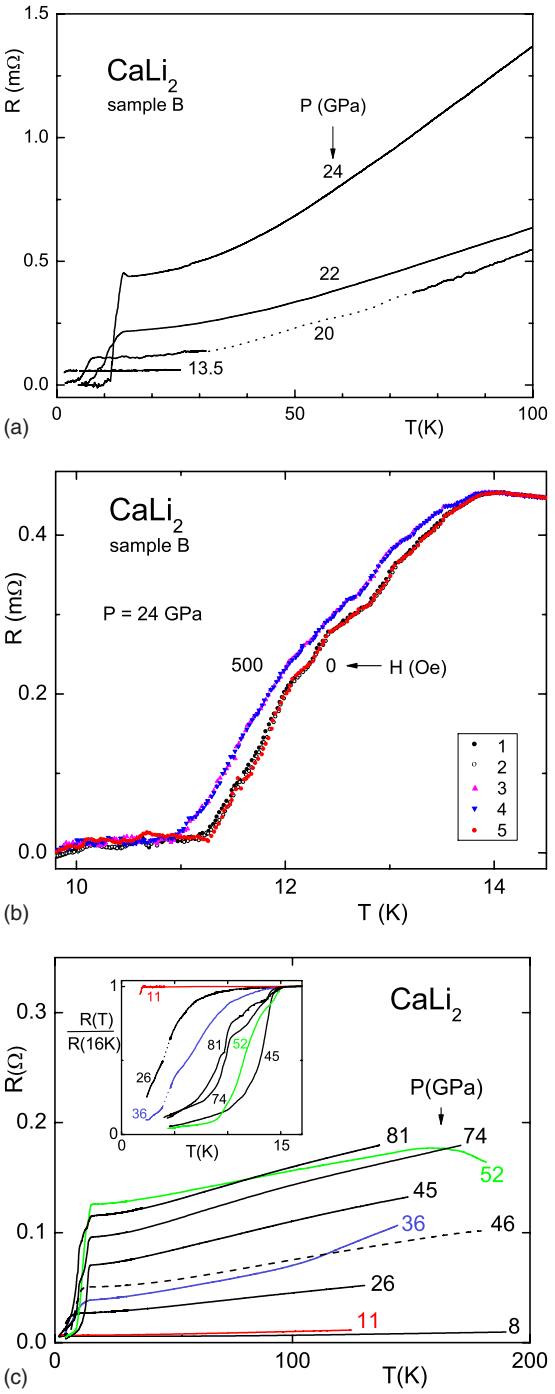

FIG. 6. (Color online) (a) Electrical resistance versus temperature for $CaLi_2$ (sample B) at 13.5, 20, 22, and 24 GPa pressure, measured in that order; dashed line fills in gap in data at 20 GPa; (b) shift in superconducting transition of sample B at 24 GPa under 500 Oe magnetic field, numbers giving order of measurement; (c) resistance versus temperature for sample A at 8, 11, 26, 36, 45, 52, 74, 81, and 46 GPa, measured in that order. Inset shows data plotted as resistance normalized at 16 K versus temperature to 17 K; dots bridge gap in data at 26 and 36 GPa. Figure 6(c) is reproduced from Ref. 18.

The sharp drop in the resistivity near 10 K seen in the high-pressure data for $P \geq 11$ GPa in Fig. 6(c) signals a superconducting transition which is seen to initially increase

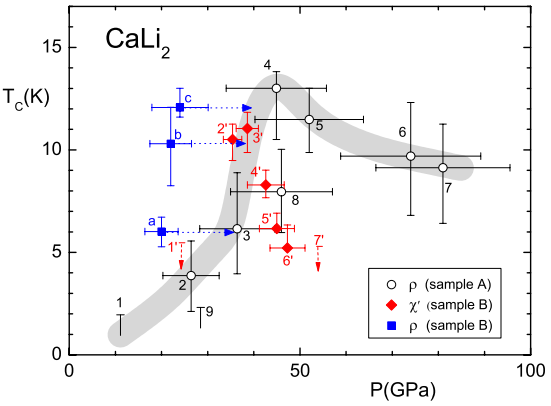

FIG. 7. (Color online) Superconducting transition temperature T_c of $CaLi_2$ versus pressure from resistivity and ac susceptibility measurements in Figs. 6 and 8. Value of T_c is determined from transition midpoint; vertical error bars give 20%–80% transition width. Horizontal error bars reflect width of R_1 ruby peak. Numbers and letters give order of measurement. Horizontal dashed lines with arrows indicate a correction of the estimated pressure from resistivity data on sample B by 15 GPa to higher pressures (see text). The broad gray line is a guide for the eyes.

with pressure but then to pass through a maximum near 45 GPa. This nonmonotonic pressure dependence is brought out in Fig. 7 where the value of T_c is defined by the midpoint of the resistive transition, the "error bars" giving the 20%–80% transition width. In a nonhydrostatic pressure environment, as in the present resistivity experiments, there is an appreciable pressure gradient across the sample, the peak pressure being at the center. In this case the resistive transition midpoint would be expected to more closely reproduce the intrinsic $T_c(P)$ dependence than, for example, the transition onset. When the intrinsic $T_c(P)$ passes through a maximum, the region of the sample responsible for the onset temperature shifts from the cell center to the cell outer with increasing pressure, thus causing $T_c^{\text{onset}}(P)$ to "hang up" at its maximum value. The difference in the pressure dependence of T_c for samples A and B in Fig. 7 is appreciable and likely arises from the fact that, unlike for sample A, the ruby sphere in the resistivity measurement on sample B was located ~ 30 μm from the sample center, thus lowering the indicated pressure by ~ 15 GPa. The horizontal blue dashed lines with arrows in Fig. 7 approximately correct for this effect. With this correction the reproducibility in $T_c(P)$ for the two resistivity experiments is quite good.

C. ac susceptibility measurements

The electrical resistivity is a very sensitive technique for detecting a superconducting transition but is unable to determine whether the superconductivity is bulk or filamentary in nature; a small concentration ($\sim 1\%$) of a superconducting filamentary phase in an otherwise nonsuperconducting sample may drive the resistivity to zero. A far superior probe for bulk superconductivity is to search for a strong diamagnetic transition in the ac susceptibility.

In the present high-pressure ac susceptibility experiments

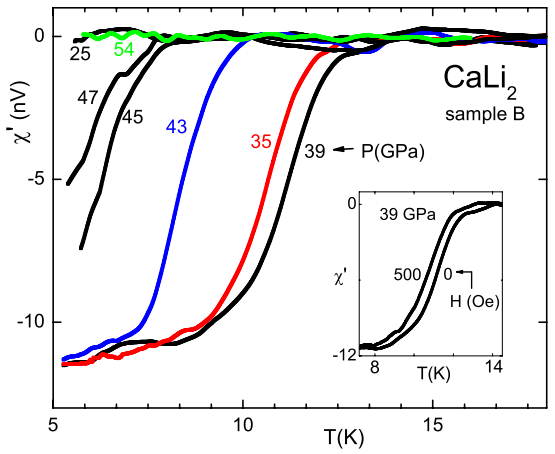

FIG. 8. (Color online) Real part of ac susceptibility versus temperature for $CaLi_2$ (sample B) for pressures 25, 35, 39, 43, 47, and 54, measured in that order. In the inset the superconducting transition for 39 GPa pressure shifts by 0.62 K to lower temperatures in 500 Oe dc magnetic field. Figure is reproduced from Ref. 18.

on $CaLi_2$, the use of a rhenium gasket, a material which superconducts under pressure at ~4 K, restricts the search for superconductivity to temperatures $T \geq 4$ K. Three separate ac susceptibility experiments were carried out in a DAC on sample A in dense He pressure medium which provides nearly hydrostatic pressure at low temperatures, the first over the pressure range to 18 GPa, the second to 30 GPa, and the third to 50 GPa; no superconductivity above 4 K was detected in these three experiments. Next, sample B was pressurized in He pressure medium to 46 GPa, with a similar negative result. The initial diameter of the gasket hole in these experiments was 235 μm. The sample size was chosen a good deal smaller $(80 \times 80 \times 20)$ (μm^3) so that under compression the sample was not directly strained by either the walls of the gasket or the culet faces of the diamond anvils.

In the next series of ac susceptibility measurements to very high pressures, the hole in the W-25% Re gasket was filled with $CaLi_2$ sample with no pressure medium added. This resulted in nonhydrostatic pressure conditions which led to appreciable plastic deformation of the sample. This nonhydrostatic technique, however, affords two principal advantages: (a) a much larger sample volume (area) is obtained so that the onset of superconductivity gives a larger diamagnetic fingerprint, and (b) the pressure conditions are similar to those in the above electrical resistivity and x-ray structure experiments.

In Fig. 8 the real part of the ac susceptibility of $CaLi_2$ is plotted versus temperature for monotonically increasing pressure.[18] Data at or below 5 K are not shown since in this temperature region the susceptibility is saturated by the overwhelming diamagnetic signal from the superconducting W-25% Re gasket. At 25 and 54 GPa no superconducting transition is observed above 5 K. However, at intermediate pressures a strong diamagnetic transition, consistent with 70%–100% flux expulsion, is seen which initially increases with pressure but passes through a maximum at $T_c \approx 12$ K near 39 GPa. As expected for a superconductor, the diamagnetic transition at 39 GPa is seen to shift by 0.62 K to lower temperatures (inset of Fig. 8) if a dc magnetic field of 500 Oe is applied. The same field shifts T_c down by 0.54 K at 35 GPa and by 0.48 K at 43 GPa.

The dependence of T_c for $CaLi_2$ on pressure is shown in Fig. 7 from the present resistivity and ac susceptibility experiments. The $T_c(P)$ dependence for the resistivity measurement on sample B, as corrected to higher pressures per the discussion above, agrees reasonably well with the parallel measurements on sample A. The shape of the maximum in $T_c(P)$ from χ' on sample B differs considerably from that of ρ on sample A. These differences are likely due to the appreciable pressure gradients across the sample and/or shear stress effects in these nonhydrostatic experiments. Since the susceptibility measurement gives a superior account of the superconducting properties in the bulk sample, the $T_c(P)$ dependence derived from it is likely closer to the true intrinsic dependence. The pronounced peak in $T_c(P)$ near 40 GPa is indicative of a structural phase transition near this pressure. Indeed, as pointed out above, the x-ray results in Figs. 3(b) and 3(c) give clear evidence for a structural transition from an hcp to orthorhombic phase which begins near 27 GPa and completes at ~46 GPa. The data indicate that both the low- and high-pressure phases are superconducting; the pressure derivative (dT_c/dP), however, is positive for the hcp phase and negative for the orthorhombic phase. The present resistivity and x-ray diffraction data give no evidence for dissociation of $CaLi_2$ under pressure; sample dissociation would be expected to lead to a sizeable increase in the residual resistivity ρ_o and marked irreversibility in the resistivity data [Fig. 5(c)], neither of which is observed.

In summary, for pressures above 11 GPa the present experiments confirm the pressure-induced superconductivity predicted by Feng *et al.*[16] for the binary compound $CaLi_2$, in analogy to the earlier findings for elemental Li and Ca. In all three materials the electrical resistivity increases sharply with pressure, in contrast to the behavior expected for simple metals with nearly free conduction electrons. The anomalous electronic properties induced under extreme pressure likely originate from the increasing localization of the conduction electrons in interstitial sites as the ion cores are brought together.[11,12,14] This transition to an anomalous metallic state is of considerable fundamental importance and can be viewed as a precursor phenomenon to the progressive breakup of the atomic shell structure of matter anticipated at astronomic pressures.

ACKNOWLEDGMENTS

The authors thank N. Ashcroft for many stimulating discussions and for suggesting these experiments. The research visit of one of the authors (T.M.) at Washington University was made possible by the Osaka University short-term student dispatch program. The authors gratefully acknowledge research support by the National Science Foundation through Grant No. DMR-0703896.

*Permanent address: KYOKUGEN, Center for Quantum Science and Technology under Extreme Conditions, Osaka University, 1-3 Machikaneyama, Toyonaka, Osaka 560-8531, Japan.

[1] J. S. Schilling, *Handbook of High Temperature Superconductivity: Theory and Experiment*, edited by J. R. Schrieffer and J. S. Brooks (Springer-Verlag, Berlin, 2007) Chap. 11; arXiv:cond-mat/0604090 (unpublished).

[2] G. J. Sizoo and H. K. Onnes, Commun. Phys. Lab. Univ. Leiden **180b** (1925).

[3] J. Tuoriniemi, K. Juntunen-Nurmilaukas, J. Uusvuori, E. Pentti, A. Salmela, and A. Sebedash, Nature (London) **447**, 187 (2007).

[4] K. Shimizu, H. Ishikawa, D. Takao, T. Yagi, and K. Amaya, Nature (London) **419**, 597 (2002).

[5] V. V. Struzhkin, M. I. Eremets, W. Gan, H. K. Mao, and R. J. Hemley, Science **298**, 1213 (2002).

[6] S. Deemyad and J. S. Schilling, Phys. Rev. Lett. **91**, 167001 (2003).

[7] T. Yabuuchi, T. Matsuoka, Y. Nakamoto, and K. Shimizu, J. Phys. Soc. Jpn. **75**, 083703 (2006).

[8] T. H. Lin and K. J. Dunn, Phys. Rev. B **33**, 807 (1986).

[9] J. S. Schilling and W. B. Holzapfel, Phys. Rev. B **8**, 1216 (1973).

[10] J. S. Schilling, High Press. Res. **26**, 145 (2006).

[11] J. B. Neaton and N. W. Ashcroft, Nature (London) **400**, 141 (1999).

[12] J. B. Neaton and N. W. Ashcroft, Phys. Rev. Lett. **86**, 2830 (2001).

[13] S. Lei, D. A. Papaconstantopoulos, and M. J. Mehl, Phys. Rev. B **75**, 024512 (2007).

[14] B. Rousseau and N. W. Ashcroft, Phys. Rev. Lett. **101**, 046407 (2008).

[15] B. Vasvari, A. O. E. Animalu, and V. Heine, Phys. Rev. **154**, 535 (1967).

[16] J. Feng, N. W. Ashcroft, and R. Hoffmann, Phys. Rev. Lett. **98**, 247002 (2007).

[17] J. Feng (private communication).

[18] T. Matsuoka, M. Debessai, J. J. Hamlin, A. K. Gangopadhyay, J. S. Schilling, and K. Shimizu, Phys. Rev. Lett. **100**, 197003 (2008).

[19] E. Hellner and F. Laves, Z. Kristallogr. **105**, 134 (1943).

[20] R. Nesper and G. J. Miller, J. Alloys Compd. **197**, 109 (1993).

[21] P. Villars and L. D. Calvert, *Pearson's Handbook of Crystallographic Data for Intermetallic Phases* (American Society for Metals, Metals Park, OH, 1985), Vol. 1, p. 368; *Pearson's Handbook of Crystallographic Data for Intermetallic Phases* (American Society for Metals, Metals Park, OH, 1985), Vol. 2, pp. 1605–1606; *Pearson's Handbook of Crystallographic Data for Intermetallic Phases* (American Society for Metals, Metals Park, OH, 1985), Vol. 3, p. 2612.

[22] To obtain the x-ray spectrum at the synchrotron facility, the sample was placed in the hole of a stainless-steel gasket in a diamond-anvil cell. The weak extra lines in the spectrum in Fig. 1(b) may arise from scattering off the gasket and other DAC addenda.

[23] J. S. Schilling, *High Pressure in Science and Technology*, MRS Symposia Proceedings No. 22 (Materials Research Society, Pittsburgh, 1984), p. 79.

[24] T. Matsuoka, S. Onoda, M. Kaneshige, Y. Nakamoto, K. Shimizu, T. Kagayama, and Y. Ohishi, J. Phys.: Conf. Ser. **121**, 052003 (2008).

[25] J. C. Chervin, B. Canny, and M. Mancinelli, High Press. Res. **21**, 305 (2001).

[26] A. D. Chijioke, W. J. Nellis, A. Soldatov, and I. F. Silvera, J. Appl. Phys. **98**, 114905 (2005).

[27] K. Shimizu, K. Amaya, and N. Suzuki, J. Phys. Soc. Jpn. **74**, 1345 (2005).

[28] M. Chai and J. M. Brown, Geophys. Res. Lett. **23**, 3539 (1996).

[29] J. J. Hamlin, V. G. Tissen, and J. S. Schilling, Phys. Rev. B **73**, 094522 (2006).

[30] T. Tomita, J. S. Schilling, L. Chen, B. W. Veal, and H. Claus, Phys. Rev. B **74**, 064517 (2006).

[31] H. D. Luedemann and G. C. Kennedy, J. Geophys. Res. **73**, 2795 (1968).

[32] D. Errandonea, R. Boehler, and M. Ross, Phys. Rev. B **65**, 012108 (2001).

[33] T. Yabuuchi, Y. Nakamoto, K. Shimizu, and T. Kikegawa, J. Phys. Soc. Jpn. **74**, 2391 (2005).

[34] F. D. Murnaghan, Proc. Natl. Acad. Sci. U.S.A. **30**, 244 (1944).

[35] M. Hanfland, I. Loa, K. Syassen, U. Schwarz, and K. Takemura, Solid State Commun. **112**, 123 (1999); M. Hanfland, K. Syassen, N. E. Christensen, and D. L. Novikov, Nature (London) **408**, 174 (2000).

[36] See, for example, J. M. Ziman, *Principles of the Theory of Solids* (Cambridge, London, 1972).

[37] A. Eiling and J. S. Schilling, J. Phys. F: Met. Phys. **11**, 623 (1981).